

# Language-Guided 3D Object Detection in Point Cloud for Autonomous Driving

Wenhao Cheng\*  
Beijing Institute of Technology  
Beijing, China

Junbo Yin\*  
Beijing Institute of Technology  
Beijing, China

Wei Li  
Inceptio  
Shanghai, China

Ruigang Yang  
Inceptio  
Shanghai, China

Jianbing Shen<sup>†</sup>  
SKL-IOTSC, CIS, University of Macau  
Macau, China

## ABSTRACT

This paper addresses the problem of 3D referring expression comprehension (REC) in autonomous driving scenario, which aims to ground a natural language to the targeted region in LiDAR point clouds. Previous approaches for REC usually focus on the 2D or 3D-indoor domain, which is not suitable for accurately predicting the location of the queried 3D region in an autonomous driving scene. In addition, the upper-bound limitation and the heavy computation cost motivate us to explore a better solution. In this work, we propose a new multi-modal visual grounding task, termed LiDAR Grounding. Then we devise a Multi-modal Single Shot Grounding (MSSG) approach with an effective token fusion strategy. It jointly learns the LiDAR-based object detector with the language features and predicts the targeted region directly from the detector without any post-processing. Moreover, the image feature can be flexibly integrated into our approach to provide rich texture and color information. The cross-modal learning enforces the detector to concentrate on important regions in the point cloud by considering the informative language expressions, thus leading to much better accuracy and efficiency. Extensive experiments on the Talk2Car dataset demonstrate the effectiveness of the proposed methods. Our work offers a deeper insight into the LiDAR-based grounding task and we expect it presents a promising direction for the autonomous driving community.

## CCS CONCEPTS

• **Computing methodologies** → **Computer vision**; **Natural language processing**; **Control methods**.

## KEYWORDS

Referring Expression Comprehension, 3D Point Cloud Detection, Multi-modal Fusion, Autonomous Driving.

## 1 INTRODUCTION

The referring expression comprehension (REC) [42, 48, 49, 53, 55, 60] task has gained increasing attention recently. The goal of REC is to localize a targeted region in a visual scene described by a natural language expression. Meanwhile, great advances have been made in autonomous driving [4, 16, 43, 62]. An intuitive idea is to explore the application of REC in autonomous driving scenarios. In this circumstance, a natural language instruction or command can

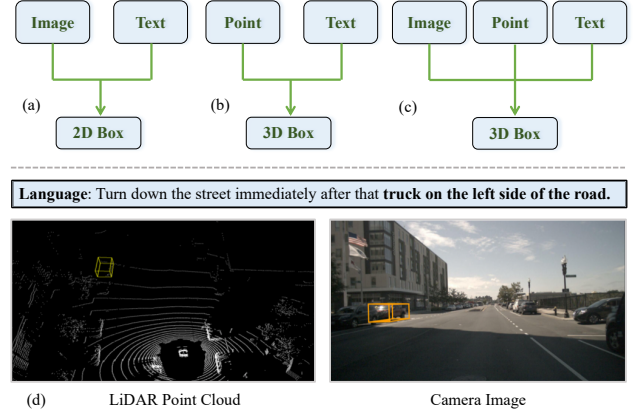


**Figure 1: Compared to the previous paradigms like (a) and (b), we propose a new multi-modal setting (c) for visual grounding in autonomous driving. An example is given in (d), which aims to ground the language referred truck in a LiDAR point cloud scene. The camera image could be optional input to provide context-rich information.**

be sent to the self-driving car to be understood and executed (e.g., park the car next to the pedestrian on the right). This is of great significance to human-car interaction and makes the autonomous driving system more user-friendly. To achieve this, an essential step is to enable the self-driving car to accurately localize the referred region in a 3D LiDAR point cloud scene.

One line literature in outdoor scene, as shown in Figure 1 (a), Talk2Car [13] is the pioneering work in this field. It proposed the first REC dataset in the autonomous driving setting based on nuScenes [4], which contains commands annotated in natural language expression for self-driving cars. However, they only focus on REC in 2D images [45], *i.e.*, grounding the language to a region represented by 2D bounding box. This is not enough in autonomous driving scenarios, since a self-driving car needs to acquire accurate 3D location of the targeted instance in order to execute the given command. Another line of work, as shown in Figure 1 (b), such as Referit3D [1] and ScanRefer [6], focus on localizing 3D objects in RGB-D scans using natural language. These methods are infeasible to adapt to outdoor 3D environment. Firstly, the large-scale LiDAR point clouds are sparse, noisy, and lack of informative appearance.

\*Equal Contribution

<sup>†</sup>Corresponding author, shenjianbingcg@gmail.com

How to incorporate the language expression with point cloud representation remains under-explored. Secondly, compared with indoor domain, there are fewer common categories in outdoor scene (car, bicycle, and pedestrian), which increases the difficulty of extracting distinguishable features from natural language. Moreover, different from the 3D object detection task that handles objects with pre-defined classes, the LiDAR grounding task needs to tackle various instances in different scenes.

To this end, we propose a new 3D REC task, *i.e.*, LiDAR Grounding, to ground command in natural language to a targeted region described by a 3D bounding box. The paradigm is illustrated in Figure 1 (c). To address the aforementioned challenges, we firstly devise an intuitive baseline following Ground-By-Detection (GBD) manner. More precisely, we can apply off-the-shelf 3D object detectors to generate 3D region proposal candidates. Then we match candidate proposals with the encoded language query by a Matching Module. We find this simple pipeline achieves mediocre performance. Moreover, several limitations exist in this baseline. Firstly, it requires a separate 3D object detector and matching network, which leads to heavy computation cost. Secondly, the grounding performance largely relies on the quality of the 3D object detector, *i.e.*, it is impossible to predict the correct region if none of the candidates access the targeted region. Therefore, a Multi-modal Single Shot Grounding (MSSG) model is further proposed to handle these problems. It jointly learns the detection model and the language model in an end-to-end fashion. At inference time, it directly gives the final grounding result without any post-processing modules like Non-maximum Suppression (NMS). Such a cross-modal fusion mechanism enables the network to focus on the targeted region and largely improves the accuracy and efficiency compared with the baseline model.

Moreover, LiDAR point clouds usually contain rich geometric information about the surrounding environment, such as the position, shape, and motion of objects, etc., and images usually contain information about the appearance and texture of objects. Some approaches, such as DeepFusion [25], BEVFusion [27] and TransFusion [3] use the complementary relationship between point clouds and images to obtain more comprehensive and accurate environmental perception. We also empirically find there is usually color information in natural language commands. Therefore, We further design a multi-modal fusion module to integrate the image feature into the point cloud representation, which can flexibly incorporate the information of the point cloud, image, or natural language.

To sum up, our main contributions are as follows:

- We propose a new multi-modal visual grounding task, named LiDAR Grounding, that aims to localize a 3D region given a natural language command. To the best of our knowledge, this is the first effort to incorporate natural language with 3D LiDAR point cloud and camera image.
- A Multi-modal Single Shot Grounding (MSSG) model, with an effective and flexible token fusion method, is further proposed in a compact way by jointly learning the point cloud and language features. Furthermore, It also enables incorporating image feature to obtain rich semantic information.
- Experimental results on the Talk2Car dataset with elaborately designed evaluation metrics demonstrates the effectiveness of our proposed models. We expect this work

presents a promising direction for the autonomous driving community.

## 2 RELATED WORK

**3D Referring Expression Comprehension.** The 3D Referring Expression Comprehension (REC) task, a.k.a. 3D Visual Grounding, aims to ground a natural language to a referred object in 3D point cloud space. Referit3D [1] proposes two datasets, termed as Sr3D (machine label) and Nr3D (human label). ScanRefer [6] is introduced similarly, but focus on grounding bounding box rather than classify predicted ones. A lot of methods [6, 19, 61, 63] have been proposed to tackle this task. A common pipeline is to first generate a bunch of 3D region proposals by 3D detector [5, 33] or segmentation module [17]. Meanwhile the language expression is embedded by a Language Encoder [11]. Then the matching network links the 3D proposals to the language expression based on the similarity scores of features [6, 61], graph neural network [19], or Transformer [63]. Finally, the proposal with the highest score will be output as the grounding result. More recently, [58] proposes to use 2D image semantics to assist 3D REC. However, all these approaches only focus on in-door scenes, which have difficulty in adapting to outdoor scenes. In this paper, we explore the 3D REC in an autonomous driving setting, called LiDAR Grounding. The more noisy and sparse LiDAR point clouds as well as the sophisticated commands pose new challenges to the grounding algorithms.

**2D Referring Expression Comprehension.** The 2D Referring Expression Comprehension (REC) task [20, 21, 26, 32, 47, 64] has attracted a lot of attention and is widely discussed, which involves locating the targeted instance in 2D images queried by the given natural language expression. Most early methods [48, 49, 53, 60] follow multi-stage pipeline. They typically first extract the region proposals from 2D object detectors [15, 18, 28, 37], meanwhile abstracting the language features with a language encoder. After that, they rank the candidate proposals and adopt a multi-modal matching network to select the best matched proposal. However, such multi-stage methods usually encounter high computation cost and the upper bound of performance is largely determined by the 2D object detectors. To address these issues, Yang et al. [55] propose a fast one-stage paradigm that fuses a text query embedding into YOLOv3 [36], enabling an end-to-end optimization of the grounding model. Song et al. [42] further explore the 2D REC task in video domain and propose semantic attention learning to disentangle the referring cues from the input language expression. Built on the advances in 2D referring tasks, in this work, we tackle the LiDAR Grounding problem in the autonomous driving field.

**3D Object Detection.** Recently object detection in 3D domain has attracted a lot of research interest. We roughly categorize the approaches into two streams. Point-based methods [8, 38, 40, 56, 57] extract a set of point representation with the raw point cloud as input. Sampling and grouping [34, 35] techniques are often utilized. 3DSSD [56] also develops a fusion sampling strategy to enable high accuracy and speed. Voxel-based [23, 31, 41, 51, 52, 65] methods transform the sparse points to dense voxel representation. To improve time efficiency, sparse convolution [51] is introduced. Voxel R-CNN [12] designs voxel ROI Pooling to take full

advantage of multi-scale voxel features, achieving impressive performance. PV-RCNN [39] combines the advantages of both 3D voxel convolution and point-based abstraction, resulting a voxel-keypoint-grid pipeline, achieving remarkable gains. Recently, methods [3, 7, 9, 24, 25, 27, 30, 54] based on multi-modal fusion have achieved better performance, since images can provide rich context information. Inspired by this, we also explore the effect of image features on the proposed task.

### 3 APPROACH

In this section, we first give the definition of the LiDAR Grounding task in 3.1, and then present the baseline method grounding-by-detection in 3.2. The multi-modal single shot grounding model is illustrated in 3.3. We further present how to use image feature in 3.4.

#### 3.1 Problem Setup

We define LiDAR Grounding as a new 3D referring expression comprehension (REC) task in an autonomous driving setting. It aims to localize a region of the LiDAR point cloud described by the natural language. Formally, given a natural language expression  $Q$  with  $L$  words,  $Q = \{w_1, w_2, \dots, w_L\}$  and a point cloud scene represented as a set of 3D points,  $P = \{p_1, p_2, \dots, p_N\}$ , where  $N$  is the number of points and each  $p_i$  is a vector of 3D location coordinates  $(x, y, z)$  plus extra feature channels such as intensity measurements  $r$ . The goal is to predict a 3D bounding box  $B$  of the object referred by  $Q$ , where  $B = (u, v, d, w, l, h, \alpha)$  consists of center location  $(u, v, d)$  relative to ground plane and 3D size  $(w, l, h)$  with rotation angle  $\alpha$ .

#### 3.2 Baseline

Most existing methods [6, 19, 61, 63] for indoor referring task can be summarized as a grounding-by-detection (GBD) manner. Follow this pipeline, we firstly design a baseline for the proposed task. Fig. 2 illustrates the overview of our pipeline, which consists of two stages. Specifically, in the first stage, a bunch of 3D object region proposals are produced by an off-the-shelf 3D object detector. Then we extract the proposal features from the detector using 3D RoI pooling. In the second stage, the language expression is embedded by a Language Encoder with a GRU [11] or BERT [46]. After that, the matching network links the 3D proposals to the language expression based on the similarity scores of features. Finally, the proposal with the highest similarity scores will be output as the grounding result. Next, we will discuss each module in detail.

The 3D object detector plays a key role in the whole framework, since the final prediction is based on the candidate regions generated by it, and if the ground truth object is not covered, the subsequent work will be meaningless. Therefore, we employ a state-of-the-art 3D object detector CenterPoint [59] to extract the region proposals  $P$ :

$$P = \{p_1, p_2, \dots, p_K\} \quad (1)$$

where  $K$  is the number of proposals and each  $p_i$  is the bounding box of the candidate regions. Then, in order to extract the corresponding proposal features  $F_{p_i}$ , we attempt to fuse the features of center points along the five faces of a 3D bounding box following [59]:

$$F_{p_i} = \text{RoI}(p_i), \quad i = 1, 2, \dots, K \quad (2)$$

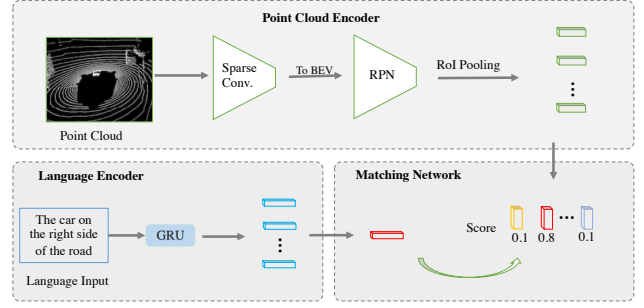


**Figure 2: Overview of the baseline model. Firstly the region proposals are extracted by a pre-trained 3D detector and processed by 3D RoI Pooling, and the language expression is encoded by a GRU. Then a Matching Network is utilized to match each candidate proposal with the language query. Finally, the one with highest score is selected as the final grounding result.**

where  $\text{RoI}$  denotes 3D RoI pooling.

As for Language Encoder, we use a bi-directional GRU to extract the linguistic feature, and just summarize the last final hidden state in the forward and backward process to get the global language feature representation  $F_t$ .

In Matching Network, we first map the point feature and language feature into the latent space:

$$\hat{F}_p = f(F_p) \quad \hat{F}_t = f(F_t) \quad (3)$$

where  $f$  means Multi-Layer Perceptrons (MLP) followed by L2 normalization to remap the feature value ranging from 0 to 1.

Finally, to measure the correlation or get the matching score between the features of each candidate region and language query, we have:

$$\text{score}_{p_i} = \cos(\hat{F}_{p_i}, \hat{F}_t), \quad i = 1, 2, \dots, K. \quad (4)$$

where  $\cos$  denotes the cosine similarity function.

During training, we select the top  $K$  region proposals based on the confidence score generated by the pre-trained detector. The proposal with highest intersect-over-union (IoU) with the ground truth box in the bird's eye view will be viewed as the positive, and other proposals are the negatives. The scenes that have all the candidate proposals with lower IOU between the ground truth box will be ignored. We freeze the Point Cloud Encoder and only update the parameters of Language Encoder and the Matching Module by minimizing the Cross Entropy Loss.

$$L = -s^* \log(s_i), \quad s_i = \text{softmax}_i(\text{score}_{p_i}) \quad (5)$$

where  $s^*$  corresponds to the binary ground truth. At inference time, the candidate proposal with the highest matching score will be selected as the final prediction.

#### 3.3 Multi-modal Single Shot Grounding

According to the experimental results in Section 4.4, the baseline model has achieved robust performance. However, there are still some limitations. First, the final performance is capped by the 3D object detector in the first stage. For example, the matching network will never give a correct answer if none of the predicted

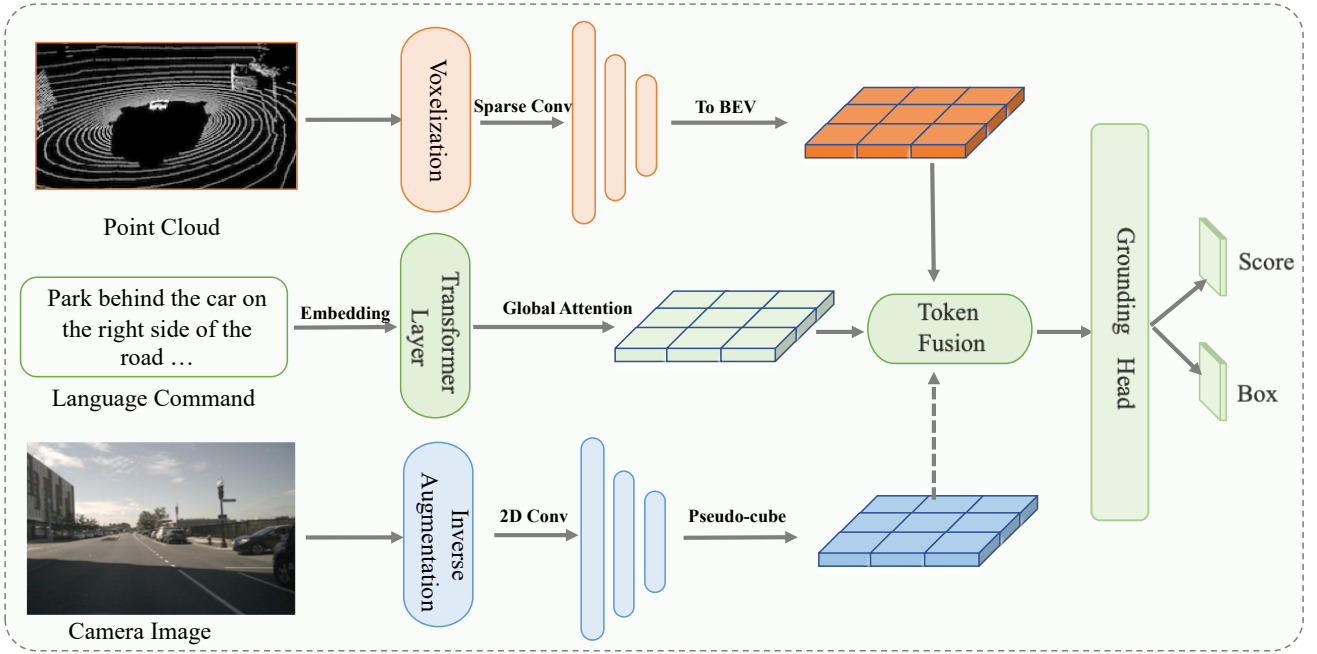


**Figure 3: Overview of our multi-modal single shot grounding model. This method enforces cross-modal feature interaction and joint optimization between point cloud and language expression representations in a single shot fashion. The image feature could be optional input to provide semantic information.**

3D region proposals have covered the targeted region. Second, the 3D object detector and matching network are separately learned, which lacks effective feature fusion and information exchange. To tackle these problems, we further present a single shot grounding (MSSG) model that enforces cross-modal feature interaction and end-to-end optimization for point cloud and language features. The pipeline is shown in Fig. 3.

**Language Encoding.** For the linguistic feature extraction, we try both BERT [46] layer and bidirectional GRU [11] to show the importance of language encoding. Here we take the former case as example to illustrate our method. Formally, given the language expression  $Q = [w_1, \dots, w_L]$ , we have:

$$[u_1, \dots, u_L] = \text{BERT}(\hat{w}_1, \dots, \hat{w}_L) \quad (6)$$

where  $\hat{w}_j = \text{embed}(w_j)$  is the embedding of  $j$ -th word in the input expression with length  $L$ , and the output  $u_j$  will contain context information. To get global feature representation, we adopt the pre-defined special token [CLS] as the fused text feature  $f_{\text{text}}$ .

**Point Encoding.** To build a representation of point cloud, we firstly voxelize the input point cloud. Subsequently, sparse convolution is performed, and multi-scale voxel-wise features are aggregated to obtain a deep feature representation. Then the height and channel dimension will be concatenated to get the bird’s eye view (BEV) features. In this way, we obtain the point cloud features  $f_{\text{point}}$  of a scene.

**Cross-modal Fusion.** Next, we combine the information from the point cloud branch and the language branch. We first map the language features and point features to a latent embedding space, then the element-wise product gives the cross-modal features.

Formally, we have:

$$f_x = (f_{\text{text}} W_t) \odot (g(f_{\text{point}})) \quad (7)$$

where  $W_t$  is learnable parameter, and  $g$  represents  $1 \times 1$  2D convolution followed by batch normalization and ReLU. The language embedding will automatically broadcast to integrate into the point cloud feature space. Due to the sparsity of 3D LiDAR point clouds, 2D convolutions are often utilized to enrich feature representation. Inspired by the success of vision transformers [14, 29, 50], we adopt Window-based self Attention (WSA) to get a transformed feature. In each WSA block, we have:

$$\begin{aligned} U &= X_{i-1} + \text{Attn}(X_{i-1}) \\ X_i &= \text{LN}(U + \text{MLP}(\text{LN}(U))) \end{aligned} \quad (8)$$

where  $X_{i-1}$  represents the output feature from previous layer, LN means layer normalization [2], Attn denotes the scaled dot-product attention [46], and MLP is the Multi-Layer Perceptron. Specially, in the MLP, we add a layer of  $3 \times 3$  convolution to increase the receptive field.

**Grounding Head.** Finally, the fused features  $f_x$  are fed into a center-based head to predict the bounding box and confidence score. The general 3D object detector like Centerpoint [59] utilizes a  $K$ -channel heatmap head for each of  $K$  classes to generate a heatmap peak at the center of any detected object, optimized by Focal Loss [28]. However, in response to the proposed task, only one object instance provides positive supervised signal. The  $K$ -channel heatmap may contain a lot of redundant information and even impair the performance. Thus, we reduce the channel size into one to predict the confidence score of the referred object across all

classes. As for the regression head, we use four separate sub-heads to predict the 2D center relative to the ground plane, 3D height, 3D size and rotation angle.

**Negatives Sampling in Training.** During the process of label assignment, only the location at ground truth object center will be assigned label 1, and the others will be labeled 0, since we only select one bounding box as the final result. However, the large spatial size of heat map *i.e.*,  $180 \times 180$  raises another issue. Different from 2D referring tasks [21, 42, 53], the image can be downsampled to small scales, such as  $7 \times 7$  or  $13 \times 13$ . The large heatmap will bring too many negative samples, which may dominate the gradient propagation. To address this issue, we propose a binary mask map (BMM) to reduce the ratio of negatives. Only the locations with mask 1 will be taken into account for the gradients. Formally, the confidence score of location  $(i, j)$  is calculated by:

$$p(i, j) = \frac{b(i, j) \exp(h(i, j))}{\sum_{x, y} b(x, y) \exp(h(x, y))} \quad (9)$$

where  $b(x, y)$  is the value of binary mask map at location  $(x, y)$  and  $h(x, y)$  is the output logit confidence of heat map.

In our implementation, we use a simple but effective method to get BMM. Specifically, we randomly sample the negatives with probability  $\gamma$ . At each location, it has probability  $\gamma$  to be masked with 1. Particularly, it is guaranteed that the location of ground truth region center must be masked. We refer to the experiment part Section 4.4 for the analysis of BMM.

**Training.** During training, the confidence loss function is defined as follows:

$$L_{conf} = - \sum_{i, j} g_{i, j} \log(p_{i, j}) \quad (10)$$

where  $g_{i, j}$  is the assigned label and  $p_{i, j}$  is the output confidence score at location  $(i, j)$ . And the regression loss can be formulated by:

$$L_{reg} = l(o, o^*) \quad (11)$$

where  $l$  represents L1 loss, and  $o$  denotes the attributes of output bounding box at ground truth center  $o^*$ , including 3D center location, 3D size, sine and cosine value of yaw angle.

At last, we have the total training loss:

$$L_{total} = L_{conf} + \lambda L_{reg} \quad (12)$$

where  $\lambda$  is the weighting coefficient.

### 3.4 Multi-Modal Fusion

Inspired by previous multi-modal fusion methods [3, 9, 10, 24, 25, 27, 30, 54], we explore the effectiveness of image feature on the proposed task. Based on the fact that the object detection is very similar to the task proposed in this paper. The obvious difference is that the LiDAR Grounding only detects one candidate area, while the object detection task needs to detect all objects, but their shared features are similar. Therefore, an intuitive idea is that if the object detection task can benefit from image features, then the proposed task can also learn from this idea. In this way, the MSSG model can utilize the information of point cloud, natural language and camera image simultaneously.

**Token Fusion.** We explore the scheme of fusion in the BEV space, that is to say, the features in the three modals of point cloud, language and image will be initially encoded by their own independent

encoders, and then the information of each modal will be exchanged in the middle stage to carry out effective fusion. Adopting such a method has the following advantages. First, some pre-trained models can be used to introduce prior information to improve the performance of the model. Second, after the initial encoding by the encoders of the respective modalities, the feature representation of each modality is enriched, and a clearer understanding of its own meaning is obtained, and then in the process of interacting with information from other modalities, it is also easier to know what they need and what they can provide, thus lead to better fusion effect. The whole process can be termed as token fusion, and expressed as:

$$\begin{aligned} \hat{L} &= F_l(L) \\ \hat{P} &= F_p(P) \\ \hat{I} &= F_i(I) \\ X &= G([\hat{L}; \hat{P}; \hat{I}]) \end{aligned} \quad (13)$$

Where  $L, P, I$  respectively represent the initial input language, point cloud and image features, and  $F_l$  represents the language encoder. Recently, there are many language models based on Transformer that are pre-trained on large-scale datasets emerging. This approach can conveniently benefit from developments in the corresponding field.  $F_p$  represents the encoder of the point cloud, here it can use the backbone network for 3D object detection with the best performance, or the pre-trained network on other datasets.  $F_i$  represents the encoder of the picture, which can use either a traditional two-dimensional convolution-based network or a recent advanced Transformer-based model.  $G$  represents a module that fuses the features of the three modalities. Here, it is represented by concatenating. In addition, point-by-point addition, multiplication, or other fusion methods using attention mechanisms can also be used. Then the fused feature  $X$  can be used for downstream detection tasks.

In our implementation, we use a pre-trained ResNet-152 [18] as the image encoder. After the image features are aligned with the point cloud, a pseudo-cube will be filled in as a pseudo-point cloud, which will be in one-to-one correspondence with the previous point cloud features to facilitate subsequent fusion operations in equation 7.

**Inverse Augmentation.** During specific training process, data augmentation is often used to improve data efficiency, such as flip, rotation and translation. However, these transformation of point cloud is random and changes its original location in 3D space. It is necessary to align the image and point cloud features. Therefore, we record the augmentation details of point cloud and perform the same transformation in 2D image.

## 4 EXPERIMENTAL RESULTS

### 4.1 Dataset

We evaluate the proposed methods on Talk2Car dataset [13] which is built upon the nuScenes dataset [4], a large-scale dataset for autonomous driving. The Talk2Car dataset contains 11,959 commands of 850 videos. Each command describes one target region in a frame and consists of 11.01 words, 2.32 nouns, 2.29 verbs and 0.62 adjectives on average. It has fine-grained classes the same as

Type	car	truck	c.v.	bus	trailer	barrier	motorcycle	bicycle	pedestrian	t.c.
A	0.5	0.5	0.5	0.5	0.5	0.25	0.25	0.25	0.25	0.25
B	0.7	0.7	0.7	0.7	0.7	0.5	0.5	0.5	0.3	0.3

**Table 1: Two types of designed IoU setting. The c.v. means construction vehicle and t.c. denotes traffic cone.**

Method	BEV AP		3D AP	
	@A	@B	@A	@B
Talk2Car* [13]	30.6	24.4	27.9	19.1
MSSG (Ours)	37.8	26.1	31.9	20.3
MSSG + Pre (Ours)	48.0	34.1	43.0	22.4
MSSG + Pre + Img (Ours)	<b>50.1</b>	<b>35.7</b>	<b>45.4</b>	<b>23.7</b>

**Table 2: Comparison of performance with different methods on Talk2Car [13] Validation Set. Pre represents pre-training, Img means image features, and \* denotes our re-implementation.**

nuScenes, with 23 categories of different vehicles, pedestrians, mobility devices and others. The dataset is split into train, validation and test sets with a number of 8,349, 1,163 and 2,447 commands, respectively. It has 3D bounding box annotations, but the box is annotated in the camera front view. Therefore, to get the box under point cloud, we convert the original box into LiDAR-top view using the corresponding calibrated parameters. Specifically, we firstly transform the box in camera view to ego view. Secondly, the ego vehicle frame for the timestamp of the image is converted into global plane. Thirdly, transform the global frame to ego view in LiDAR-top. Finally, the LiDAR box can be obtained according to the time step of the sweep. In each step, the translation and rotation angle will be transformed at the same time. Since the test set is unavailable, we only conduct the experiments on the train and validation set.

## 4.2 Evaluation Metrics

We use the average precision (AP) as the evaluation metric. The match in BEV is defined by thresholding the Intersection-over-Union (IoU) between the predicted box and the ground truth in the bird eye view. The 3D AP further considers the accuracy of box height. The prediction is correct when the IoU is larger than a certain threshold. Due to the large scale variance of different object instance, we design two types of IoU threshold setting to evaluate the model performance. Following the nuScenes [4] detection task, we merge similar classes as well, resulting in 10 super classes. Specifically, the IoU threshold is presented in Table 1. Our motivation for setting two different types of thresholds is to show the accuracy of the box regression. Since in the process of inference, we only select the bounding box with the highest score as the final result. On the other hand, the volume of different objects in the dataset is quite different, and it is unreasonable to only set a unified threshold as the evaluation metric.

IoU Type	Training			Validation		
	Found	Total	Ratio	Found	Total	Ratio
A	5058	8328	0.61	643	1128	0.57
B	4056	8328	0.49	523	1128	0.46

**Table 3: Statistics of the proportion that covers ground truth in proposals generated by pre-trained CenterPoint [59].**

Model	Component			NDS	mAP
	Base	Img	Aug		
1	✓			43.4	32.6
2	✓	✓		44.0	34.2
3	✓		✓	47.5	41.8
4	✓	✓	✓	47.6	42.2

**Table 4: Ablation study showing the effectiveness of image feature in object detection on 1/4 NuScenes [4] dataset. Img represents image feature, and Aug means data augmentation.**

## 4.3 Implementation Details

For the baseline method, we extend the Talk2Car [13] approach in a 3D manner. Specially, in terms of the Point Cloud Encoder, we pre-train a two-stage CenterPoint [59] with VoxelNet [65] as backbone on nuScenes [4] following original setting [59]. The number of selected region proposals is set to  $K = 128$ . The Language Encoder uses Bi-GRU with a 512 hidden size. In Matching Network, the dimension of latent space is set to 512. We train the model for 20 epochs with a batch size of 4. The stochastic gradient descent (SGD) is used with momentum 0.9, weight decay  $1e-4$  and initial learning rate 0.01 with a drop rate of 0.1 at 16-th epoch.

For the proposed single shot grounding (MSSG) approach, the window size in WSA block is set to 9, and we use 2 blocks for time efficiency. For the language encoder, we just use 2 layers of BERT for a relatively fair comparison. Since the ground truth regions only appear in the camera front view, we filter the point clouds, leaving only those that can be projected into the image of the camera front sensor. We only use global scaling and translation as the augmentation method. The weighting coefficient  $\lambda$  is set to 0.25. In terms of the training details, we use Adam [22] optimizer to train the model for 20 epochs with batch size 4. We use one-cycle learning rate policy [44], with max learning rate  $1e-3$ , weight decay 0.01, and momentum from 0.85 to 0.95. When utilizing pre-training method, we design a simple detection head for MSSG, then we train the new model on NuScenes training set to acquire some prior knowledge. The pre-trained network weights are used to initialize the backbone of the original MSSG.

## 4.4 Results

**Overall Performance.** Table 2 shows the overall performance of the proposed methods on Talk2Car [13] validation set. We report the average precision (AP) over all classes under two types of

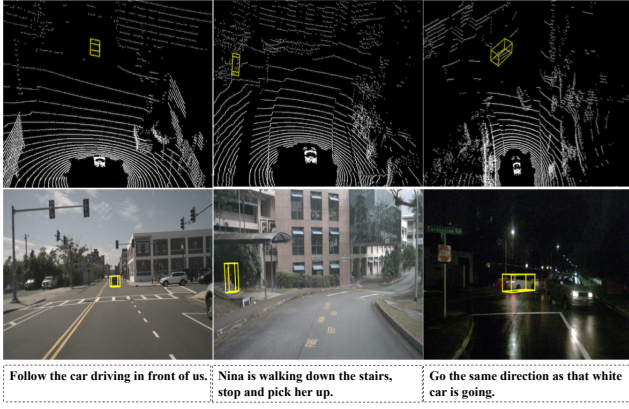


**Figure 4: Three correct examples inferred by MSSG on Talk2Car validation set. Grounded 3D bounding boxes are shown in yellow.**

IoU setting, where @A means *Type-A* and @B represents *Type-B*. From the table, we can find that the single shot grounding (MSSG) method significantly surpasses the grounding-by-detection (baseline) method. Our MSSG surpassed the baseline by 7.2% under type-A setting in BEV space, 4.0% in 3D space, which demonstrates the significant effectiveness of rich cross-modal feature interaction of MSSG pipeline. Moreover, when the MSSG adopts the pre-trained backbone, the performance gets significant improvement, i.e., 10.2% in BEV-AP@A and 11.1 % of 3D-AP@A. Since the setting B that has a higher IoU threshold, there is an interesting phenomenon. The boost in condition B is relatively small compared with A. In other words, the baseline is more robust to evaluation metrics. This can be attributed to the off-the-shelf 3D detector. Since the quality of the region proposal is fixed, it is not sensitive to different IoU thresholds. More generally, it heavily depends on the performance of the pre-trained detector, but the MSSG approach learns feature representation from scratch, and the performance of the regression head may be slightly weak, resulting in inaccurate 3D box prediction.

**Upper-bound of Baseline Method.** Table 3 shows the ratio of positive bounding box in the proposals generated by the pre-trained 3D detector CenterPoint, i.e., exists a proposal which the IoU between the predicted box and the ground truth object is larger than the corresponding threshold. To a certain degree, the ratio can represent the upper-bound of the performance of the baseline method. Since if none of the candidates could cover the ground truth area, then it is impossible that the correct region will be ranked first in the second stage. Although the baseline has acceptable result, it helplessly has a clear upper bound on performance. To improve its performance in the future, maybe a more effective method is to consider enhancing the performance of the first-stage 3D detector.

**Negatives Sampling.** Directly predicting the bounding box score at each location of large scale feature map will bring too many negative samples. To address this issue, we propose a binary mask map to sample some negatives. At each location, it has probability  $\gamma$  to be set to one. To reveal the effectiveness of  $\gamma$ , we have done sensitivity analysis with different sampling ratio on validation set.

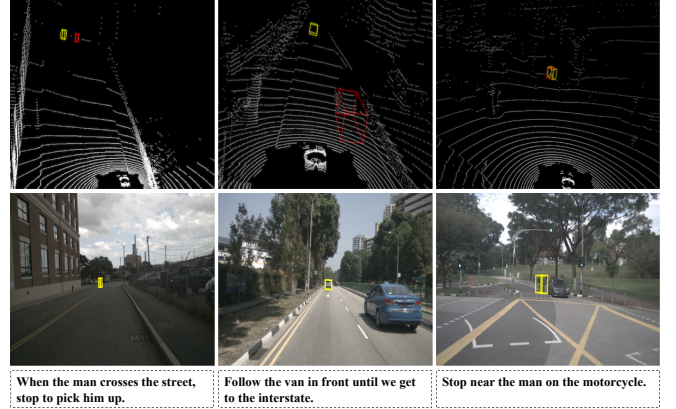


**Figure 5: Three failed cases inferred by MSSG on Talk2Car validation set. The wrong predictions are shown in red color, while the ground truth boxes are visualized in yellow.**

In our experiment, we find when the sampling ratio ranges from 0.1 to 0.4, the performance will be better than those from 0.5 to 1.0. This indicates that the model performance can benefit from reducing the number of negative examples appropriately. However, if the number of sampled negative examples is particularly small, the gradients at many positions can not be back-propagated, which may disrupt the training process. This can be demonstrated from that the best performance is achieved when the sampling ratio equals 0.4.

**Effectiveness of Image Feature.** To enhance the interaction of cross-modal features, we further fuse the point cloud and image features. To reveal the effectiveness of image feature, we firstly conduct a pilot experiment. As shown in Table 4, we select the Centerpoint as the baseline, trained the model on 1/4 nuScenes dataset for time efficiency. When compare model #1 and #2, the NDS is improved 0.6% and mAP is improved 1.6%, which indicates the image feature can enrich the point cloud representation. In practical training setting, data augmentation is often used to improve data efficiency. However, the transformation of point cloud is random and changes its original location in 3D space. It is necessary to align the image and point features. Therefore, we record the augmentation details of point cloud and perform the same transformation in 2D image. From the table, we can find the performance still have gains when compared model #3 with #4. The pilot experiment shows the believable benefit of image feature, then we apply the same fusion method in our MSSG model. As shown in Table 2, we can find the image feature also boosts a lot, which indicates that the model’s understanding of location information can be strengthened by deep cross-modal feature fusion. This also indicates the researchers can explore more powerful fusion module in future work.

**Qualitative Results** Fig. 4 depicts the visualization results of single shot grounding model on Talk2Car validation set, which shows the impressive results of our method. Nevertheless, the overall performance of our method is still not high (50% BEV-AP@A), so we also visualize some bad cases in Fig. 5 to ask for directions that can improve the performance. For the first failed case, long-distance localization is the major difficulty. The model has inferred that the

pedestrian needs to be located, but the long-distance target is too small to be successfully located. For the second case, the interference of multiple targets should be the most important issue. In other words, the model does not understand the language query well. As discussed before, the model tends to predict salient objects. Therefore, how to enhance the model's anti-interference is an important point. For the third case, the model is only one step away from success. Unfortunately the location predictions are not accurate. This indicates that the regression head of the model needs to be strengthened. This also reflects the benefits of setting two different types of thresholds from the side. Overall, we hope there is progress and improvement for long-distance targets, semantic understanding, and precise location regression in future work.

## 5 CONCLUSION

In this paper, we proposed a new task in the autonomous driving scenario, *i.e.*, LiDAR Grounding, that aims to ground a natural language command to the referred region in LiDAR point clouds. To tackle this task, we firstly summarize previous efforts into a new baseline, grounding-by-detection model. This method follows a two-stage pipeline: first detection and then grounding. It extracts language features and region proposal features separately, and selects the grounding result according to the similarity score generated by another matching network. We also propose an end-to-end method, sing shot grounding (MSSG) model. It enables end-to-end optimization and is more fast and accurate, thanks to the cross-modal feature interaction and fusion. We also explore the effectiveness of image feature, which has rich semantic information, leading to better performance. Extensive experiments on the Talk2Car dataset show solid results. We hope our work could present a promising direction in the autonomous driving community.

## REFERENCES

- [1] Panos Achlioptas, Ahmed Abdelreheem, Fei Xia, Mohamed Elhoseiny, and Leonidas Guibas. 2020. ReferIt3d: Neural listeners for fine-grained 3d object identification in real-world scenes. In *European Conference on Computer Vision*. Springer, 422–440.
- [2] Jimmy Lei Ba, Jamie Ryan Kiros, and Geoffrey E Hinton. 2016. Layer normalization. *arXiv preprint arXiv:1607.06450* (2016).
- [3] Xuyang Bai, Zeyu Hu, Xinge Zhu, Qingqiu Huang, Yilun Chen, Hongbo Fu, and Chiew-Lan Tai. 2022. Transfusion: Robust lidar-camera fusion for 3d object detection with transformers. In *Proceedings of the IEEE/CVF Conference on Computer Vision and Pattern Recognition*. 1090–1099.
- [4] Holger Caesar, Varun Bankiti, Alex H. Lang, Sourabh Vora, Venice Erin Liong, Qiang Xu, Anush Krishnan, Yu Pan, Giancarlo Baldan, and Oscar Beijbom. 2020. nuScenes: A Multimodal Dataset for Autonomous Driving. In *Proceedings of the IEEE/CVF Conference on Computer Vision and Pattern Recognition (CVPR)*.
- [5] R Charles, Y Li, S Hao, and J Pointnet+ Leonidas. 2017. Deep hierarchical feature learning on point sets in a metric space. *Proceedings of the Advances in Neural Information Processing Systems, Long Beach, CA, USA (2017)*, 4–9.
- [6] Dave Zhenyu Chen, Angel X Chang, and Matthias Nießner. 2020. Scanrefer: 3d object localization in rgb-d scans using natural language. In *Computer Vision—ECCV 2020: 16th European Conference, Glasgow, UK, August 23–28, 2020, Proceedings, Part XX 16*. Springer, 202–221.
- [7] Xuanyao Chen, Tianyuan Zhang, Yue Wang, Yilun Wang, and Hang Zhao. 2022. Futr3d: A unified sensor fusion framework for 3d detection. *arXiv preprint arXiv:2203.10642* (2022).
- [8] Yilun Chen, Shu Liu, Xiaoyong Shen, and Jiaya Jia. 2019. Fast point r-cnn. In *Proceedings of the IEEE/CVF International Conference on Computer Vision*. 9775–9784.
- [9] Zehui Chen, Zhenyu Li, Shiquan Zhang, Liangji Fang, Qinhong Jiang, and Feng Zhao. 2022. Autoalignv2: Deformable feature aggregation for dynamic multi-modal 3d object detection. *arXiv preprint arXiv:2207.10316* (2022).
- [10] Wenhao Cheng, Xingping Dong, Salman Khan, and Jianbing Shen. 2022. Learning Disentanglement with Decoupled Labels for Vision-Language Navigation. In *Computer Vision—ECCV 2022: 17th European Conference, Tel Aviv, Israel, October 23–27, 2022, Proceedings, Part XXXVI*. Springer, 309–329.
- [11] Junyoung Chung, Caglar Gulcehre, KyungHyun Cho, and Yoshua Bengio. 2014. Empirical evaluation of gated recurrent neural networks on sequence modeling. *arXiv preprint arXiv:1412.3555* (2014).
- [12] Jiajun Deng, Shaoshuai Shi, Peiwei Li, Wengang Zhou, Yanyong Zhang, and Houqiang Li. 2021. Voxel R-CNN: Towards High Performance Voxel-based 3D Object Detection. In *Proceedings of the AAAI Conference on Artificial Intelligence*, Vol. 35. 1201–1209.
- [13] Thierry Deruyttere, Simon Vandenhenne, Dusan Grujicic, Luc Van Gool, and Marie Francine Moens. 2019. Talk2Car: Taking Control of Your Self-Driving Car. In *Proceedings of the 2019 Conference on Empirical Methods in Natural Language Processing and the 9th International Joint Conference on Natural Language Processing (EMNLP-IJCNLP)*. 2088–2098.
- [14] Alexey Dosovitskiy, Lucas Beyer, Alexander Kolesnikov, Dirk Weissenborn, Xi-aohua Zhai, Thomas Unterthiner, Mostafa Dehghani, Matthias Minderer, Georg Heigold, Sylvain Gelly, et al. 2020. An image is worth 16x16 words: Transformers for image recognition at scale. *arXiv preprint arXiv:2010.11929* (2020).
- [15] Kaiwen Duan, Song Bai, Lingxi Xie, Honggang Qi, Qingming Huang, and Qi Tian. 2019. Centernet: Keypoint triplets for object detection. In *Proceedings of the IEEE/CVF International Conference on Computer Vision*. 6569–6578.
- [16] Andreas Geiger, Philip Lenz, Christoph Stiller, and Raquel Urtasun. 2013. Vision meets robotics: The kitti dataset. *The International Journal of Robotics Research* 32, 11 (2013), 1231–1237.
- [17] Benjamin Graham, Martin Engelcke, and Laurens Van Der Maaten. 2018. 3d semantic segmentation with submanifold sparse convolutional networks. In *Proceedings of the IEEE conference on computer vision and pattern recognition*. 9224–9232.
- [18] Kaiming He, Xiangyu Zhang, Shaoqing Ren, and Jian Sun. 2016. Deep residual learning for image recognition. In *Proceedings of the IEEE conference on computer vision and pattern recognition*. 770–778.
- [19] Pin-Hao Huang, Han-Hung Lee, Hwann-Tzong Chen, and Tyng-Luh Liu. 2021. Text-Guided Graph Neural Networks for Referring 3D Instance Segmentation. In *Proceedings of the AAAI Conference on Artificial Intelligence*, Vol. 35. 1610–1618.
- [20] Tianrui Hui, Shaoqi Huang, Si Liu, Zihan Ding, Guanbin Li, Wenguan Wang, Jizhong Han, and Fei Wang. 2021. Collaborative Spatial-Temporal Modeling for Language-Queried Video Actor Segmentation. In *Proceedings of the IEEE/CVF Conference on Computer Vision and Pattern Recognition*. 4187–4196.
- [21] Ya Jing, Tao Kong, Wei Wang, Liang Wang, Lei Li, and Tieniu Tan. 2021. Locate Then Segment: A Strong Pipeline for Referring Image Segmentation. In *Proceedings of the IEEE/CVF Conference on Computer Vision and Pattern Recognition (CVPR)*. 9858–9867.
- [22] Diederik P. Kingma and Jimmy Ba. 2015. Adam: A Method for Stochastic Optimization. In *3rd International Conference on Learning Representations, San Diego, CA, USA, May 7–9, 2015, Conference Track Proceedings*.
- [23] Alex H Lang, Sourabh Vora, Holger Caesar, Lubing Zhou, Jiong Yang, and Oscar Beijbom. 2019. Pointpillars: Fast encoders for object detection from point clouds. In *Proceedings of the IEEE/CVF Conference on Computer Vision and Pattern Recognition*. 12697–12705.
- [24] Yanwei Li, Yilun Chen, Xiaojuan Qi, Zeming Li, Jian Sun, and Jiaya Jia. 2022. Unifying voxel-based representation with transformer for 3d object detection. *arXiv preprint arXiv:2206.00630* (2022).
- [25] Yingwei Li, Adams Wei Yu, Tianjian Meng, Ben Caine, Jiquan Ngiam, Daiyi Peng, Junyang Shen, Yifeng Lu, Denny Zhou, Quoc V Le, et al. 2022. Deepfusion: Lidar-camera deep fusion for multi-modal 3d object detection. In *Proceedings of the IEEE/CVF Conference on Computer Vision and Pattern Recognition*. 17182–17191.
- [26] Chen Liang, Yu Wu, Tianfei Zhou, Wenguan Wang, Zongxin Yang, Yunchao Wei, and Yi Yang. 2021. Rethinking Cross-modal Interaction from a Top-down Perspective for Referring Video Object Segmentation. *arXiv preprint arXiv:2106.01061* (2021).
- [27] Tingting Liang, Hongwei Xie, Kaicheng Yu, Zhongyu Xia, Zhiwei Lin, Yongtao Wang, Tao Tang, Bing Wang, and Zhi Tang. 2022. Bevfusion: A simple and robust lidar-camera fusion framework. *arXiv preprint arXiv:2205.13790* (2022).
- [28] Tsung-Yi Lin, Priya Goyal, Ross Girshick, Kaiming He, and Piotr Dollar. 2017. Focal Loss for Dense Object Detection. In *Proceedings of the IEEE International Conference on Computer Vision (ICCV)*.
- [29] Ze Liu, Yutong Lin, Yue Cao, Han Hu, Yixuan Wei, Zheng Zhang, Stephen Lin, and Baining Guo. 2021. Swin transformer: Hierarchical vision transformer using shifted windows. In *Proceedings of the IEEE/CVF International Conference on Computer Vision*. 10012–10022.
- [30] Zhijian Liu, Haotian Tang, Alexander Amini, Xinyu Yang, Huizi Mao, Daniela Rus, and Song Han. 2022. BEVFusion: Multi-Task Multi-Sensor Fusion with Unified Bird's-Eye View Representation. *arXiv preprint arXiv:2205.13542* (2022).
- [31] Zhe Liu, Xin Zhao, Tengpeng Huang, Ruolan Hu, Yu Zhou, and Xiang Bai. 2020. Tanet: Robust 3d object detection from point clouds with triple attention. In *Proceedings of the AAAI Conference on Artificial Intelligence*, Vol. 34. 11677–11684.
- [32] Gen Luo, Yiwei Zhou, Xiaoshuai Sun, Liujuan Cao, Chenglin Wu, Cheng Deng, and Rongrong Ji. 2020. Multi-Task Collaborative Network for Joint Referring

- Expression Comprehension and Segmentation. In *Proceedings of the IEEE/CVF Conference on Computer Vision and Pattern Recognition (CVPR)*.
- [33] Charles R Qi, Or Litany, Kaiming He, and Leonidas J Guibas. 2019. Deep hough voting for 3d object detection in point clouds. In *Proceedings of the IEEE/CVF International Conference on Computer Vision*. 9277–9286.
- [34] Charles R Qi, Hao Su, Kaichun Mo, and Leonidas J Guibas. 2017. Pointnet: Deep learning on point sets for 3d classification and segmentation. In *Proceedings of the IEEE conference on computer vision and pattern recognition*. 652–660.
- [35] Charles Ruizhongtai Qi, Li Yi, Hao Su, and Leonidas J Guibas. 2017. Pointnet++: Deep hierarchical feature learning on point sets in a metric space. *Advances in neural information processing systems* 30 (2017).
- [36] Joseph Redmon and Ali Farhadi. 2018. Yolov3: An incremental improvement. *arXiv preprint arXiv:1804.02767* (2018).
- [37] Shaoqing Ren, Kaiming He, Ross Girshick, and Jian Sun. 2015. Faster r-cnn: Towards real-time object detection with region proposal networks. *Advances in neural information processing systems* 28 (2015), 91–99.
- [38] Shaoshuai Shi, Chaoxu Guo, Li Jiang, Zhe Wang, Jianping Shi, Xiaogang Wang, and Hongsheng Li. 2020. Pv-rcnn: Point-voxel feature set abstraction for 3d object detection. In *Proceedings of the IEEE/CVF Conference on Computer Vision and Pattern Recognition*. 10529–10538.
- [39] Shaoshuai Shi, Chaoxu Guo, Li Jiang, Zhe Wang, Jianping Shi, Xiaogang Wang, and Hongsheng Li. 2020. PV-RCNN: Point-Voxel Feature Set Abstraction for 3D Object Detection. In *Proceedings of the IEEE/CVF Conference on Computer Vision and Pattern Recognition (CVPR)*.
- [40] Shaoshuai Shi, Zhe Wang, Jianping Shi, Xiaogang Wang, and Hongsheng Li. 2020. From points to parts: 3d object detection from point cloud with part-aware and part-aggregation network. *IEEE transactions on pattern analysis and machine intelligence* 43, 8 (2020), 2647–2664.
- [41] Martin Simony, Stefan Milzy, Karl Amendey, and Horst-Michael Gross. 2018. Complex-yolo: An euler-region-proposal for real-time 3d object detection on point clouds. In *Proceedings of the European Conference on Computer Vision (ECCV) Workshops*. 0–0.
- [42] Sijie Song, Xudong Lin, Jiaying Liu, Zongming Guo, and Shih-Fu Chang. 2021. Co-Grounding Networks With Semantic Attention for Referring Expression Comprehension in Videos. In *Proceedings of the IEEE/CVF Conference on Computer Vision and Pattern Recognition (CVPR)*. 1346–1355.
- [43] Pei Sun, Henrik Kretschmar, Xerxes Dotiwalla, Aurelien Chouard, Vijaysai Patnaik, Paul Tsui, James Guo, Yin Zhou, Yuning Chai, Benjamin Caine, et al. 2020. Scalability in perception for autonomous driving: Waymo open dataset. In *Proceedings of the IEEE/CVF Conference on Computer Vision and Pattern Recognition*. 2446–2454.
- [44] Guggler Sylvain. 2018. The 1cycle policy. <https://sgugger.github.io/the-1cycle-policy.html>.
- [45] Simon Vandenhenne, Thierry Deruyttere, and Dusan Grujicic. 2020. A baseline for the commands for autonomous vehicles challenge. *arXiv preprint arXiv:2004.13822* (2020).
- [46] Ashish Vaswani, Noam Shazeer, Niki Parmar, Jakob Uszkoreit, Llion Jones, Aidan N Gomez, Lukasz Kaiser, and Illia Polosukhin. 2017. Attention is all you need. In *Proceedings of the 31st International Conference on Neural Information Processing Systems*. 6000–6010.
- [47] Hao Wang, Zheng-Jun Zha, Liang Li, Dong Liu, and Jiebo Luo. 2021. Structured Multi-Level Interaction Network for Video Moment Localization via Language Query. In *Proceedings of the IEEE/CVF Conference on Computer Vision and Pattern Recognition*. 7026–7035.
- [48] Liwei Wang, Yin Li, Jing Huang, and Svetlana Lazebnik. 2018. Learning two-branch neural networks for image-text matching tasks. *IEEE Transactions on Pattern Analysis and Machine Intelligence* 41, 2 (2018), 394–407.
- [49] Peng Wang, Qi Wu, Jiewei Cao, Chunhua Shen, Lianli Gao, and Anton van den Hengel. 2019. Neighbourhood watch: Referring expression comprehension via language-guided graph attention networks. In *Proceedings of the IEEE/CVF Conference on Computer Vision and Pattern Recognition*. 1960–1968.
- [50] Enze Xie, Wenhai Wang, Zhiding Yu, Anima Anandkumar, Jose M Alvarez, and Ping Luo. 2021. SegFormer: Simple and efficient design for semantic segmentation with transformers. *Advances in Neural Information Processing Systems* 34 (2021).
- [51] Yan Yan, Yuxing Mao, and Bo Li. 2018. Second: Sparsely embedded convolutional detection. *Sensors* 18, 10 (2018), 3337.
- [52] Bin Yang, Wenjie Luo, and Raquel Urtasun. 2018. Pixor: Real-time 3d object detection from point clouds. In *Proceedings of the IEEE conference on Computer Vision and Pattern Recognition*. 7652–7660.
- [53] Sibe Yang, Guanbin Li, and Yizhou Yu. 2019. Cross-Modal Relationship Inference for Grounding Referring Expressions. In *Proceedings of the IEEE/CVF Conference on Computer Vision and Pattern Recognition (CVPR)*.
- [54] Zeyu Yang, Jiaqi Chen, Zhenwei Miao, Wei Li, Xiatian Zhu, and Li Zhang. 2022. DeepInteraction: 3D Object Detection via Modality Interaction. In *Advances in Neural Information Processing Systems*, Alice H. Oh, Alekh Agarwal, Danielle Belgrave, and Kyunghyun Cho (Eds.).
- [55] Zhengyuan Yang, Boqing Gong, Liwei Wang, Wenbing Huang, Dong Yu, and Jiebo Luo. 2019. A Fast and Accurate One-Stage Approach to Visual Grounding. In *Proceedings of the IEEE/CVF International Conference on Computer Vision (ICCV)*.
- [56] Zetong Yang, Yanan Sun, Shu Liu, and Jiaya Jia. 2020. 3dssd: Point-based 3d single stage object detector. In *Proceedings of the IEEE/CVF conference on computer vision and pattern recognition*. 11040–11048.
- [57] Zetong Yang, Yanan Sun, Shu Liu, Xiaoyong Shen, and Jiaya Jia. 2019. Std: Sparse-to-dense 3d object detector for point cloud. In *Proceedings of the IEEE/CVF International Conference on Computer Vision*. 1951–1960.
- [58] Zhengyuan Yang, Songyang Zhang, Liwei Wang, and Jiebo Luo. 2021. SAT: 2D Semantics Assisted Training for 3D Visual Grounding. *arXiv preprint arXiv:2105.11450* (2021).
- [59] Tianwei Yin, Xingyi Zhou, and Philipp Krahenbuhl. 2021. Center-Based 3D Object Detection and Tracking. In *Proceedings of the IEEE/CVF Conference on Computer Vision and Pattern Recognition (CVPR)*. 11784–11793.
- [60] Licheng Yu, Zhe Lin, Xiaohui Shen, Jimei Yang, Xin Lu, Mohit Bansal, and Tamara L. Berg. 2018. MAttNet: Modular Attention Network for Referring Expression Comprehension. In *Proceedings of the IEEE Conference on Computer Vision and Pattern Recognition (CVPR)*.
- [61] Zhihao Yuan, Xu Yan, Yinghong Liao, Ruimao Zhang, Zhen Li, and Shuguang Cui. 2021. Instancerefer: Cooperative holistic understanding for visual grounding on point clouds through instance multi-level contextual referring. *arXiv preprint arXiv:2103.01128* (2021).
- [62] Ekim Yurtsever, Jacob Lambert, Alexander Carballo, and Kazuya Takeda. 2020. A survey of autonomous driving: Common practices and emerging technologies. *IEEE access* 8 (2020), 58443–58469.
- [63] Lichen Zhao, Daigang Cai, Lu Sheng, and Dong Xu. 2021. 3DVG-Transformer: Relation modeling for visual grounding on point clouds. In *Proceedings of the IEEE/CVF International Conference on Computer Vision*. 2928–2937.
- [64] Yang Zhao, Zhou Zhao, Zhu Zhang, and Zhijie Lin. 2021. Cascaded Prediction Network via Segment Tree for Temporal Video Grounding. In *Proceedings of the IEEE/CVF Conference on Computer Vision and Pattern Recognition*. 4197–4206.
- [65] Yin Zhou and Oncel Tuzel. 2018. VoxelNet: End-to-End Learning for Point Cloud Based 3D Object Detection. In *Proceedings of the IEEE Conference on Computer Vision and Pattern Recognition (CVPR)*.